science.sciencemag.org/content/365/6448/83/suppl/DC1

Supplementary Materials for

The great Atlantic *Sargassum* belt

Mengqiu Wang, Chuanmin Hu*, Brian B. Barnes, Gary Mitchum, Brian Lapointe, Joseph P. Montoya

*Corresponding author. Email: huc@usf.edu

Published 5 July 2019, *Science* **365**, 83 (2019)
DOI: 10.1126/science.aaw7912

This PDF file includes:

Materials and Methods
Supplementary Text
Figs. S1 to S7
Tables S1 and S2
Caption for Movie S1
References

Other Supplementary Material for this manuscript includes the following:
(available at science.sciencemag.org/content/365/6448/83/suppl/DC1)

Movie S1

Materials and Methods

Mapping *Sargassum* distributions of areal density and biomass density in the Intra-Americas Sea and Atlantic Ocean from 2000 to 2018

All relevant MODIS (MODIS-Aqua and MODIS-Terra) data covering the Intra-Americas Sea (IAS) and Atlantic Ocean from April 2000 to December 2018 were downloaded from the U.S. National Aeronautics and Space Administration (NASA) Goddard Space Flight Center to estimate the *Sargassum* monthly distributions. The large study area ($\sim 5.3 \times 10^7$ km^2) was divided into several sub-regions (comparable to the size of the Central West Atlantic, $\sim 6.7 \times 10^6$ km^2) and processed separately. Over 20,000 MODIS granules with sufficient data coverage (> 25%) were processed for each sub-region.

To estimate the *Sargassum* distributions, we downloaded the Level-0 products and merged adjacent granules before processing to Rayleigh-corrected reflectance (Rrc, dimensionless), which was then used to derive an Alternative Floating Algae Index (AFAI) designed to detect and quantify floating vegetation (*12, 40*). Similar to the original FAI (*40*), AFAI also quantifies the seaweed's red-edge reflectance (i.e., enhanced reflectance in the near-infrared (NIR) wavelengths) with tolerance to variable atmospheric and observing conditions, with a detection limit of about 0.2% of a pixel size. We first applied an automatic feature extraction approach to identify all the *Sargassum*-containing pixels, estimated their relative *Sargassum* fractional coverage in each *Sargassum*-containing pixel using a linear unmixing scheme, and then aggregated all the valid observations within each calendar month in $0.5° \times 0.5°$ grids to obtain monthly mean *Sargassum* areal density (% cover) maps (*12*). In Wang et al. (*2018*), these *Sargassum* areal density maps were converted to biomass density (kg/m^2) maps by applying the AFAI-biomass model developed from field experiments. To convert the integrated total *Sargassum* areal coverage (in km^2, assuming they are aggregated together) to total wet biomass, a conversion factor of 3.34 kg m^{-2} (*24*) determined from field measurements was used.

The observations from the coarse-resolution MODIS data have been evaluated with 30-m resolution Landsat data in several small regions, where consistent results were obtained from regions of their common coverage (*41*). Although field validation is difficult because the *Sargassum* mats often occupy partial pixels, the combination of the two MODIS sensors resulted in ~20% valid observations in every month (i.e., one valid observation every 5 days), thus minimizing the potential bias due to infrequent observations (*41*).

Modeling *Sargassum* transport and biological growth and mortality

We applied a bio-physical model (*25*) to track the *Sargassum* trajectories and their biological growth and mortality from satellite-derived or arbitrarily assumed initial *Sargassum* particle distributions. The *Sargassum* features were treated as Lagrangian particles forced by the surface currents and 1% of the winds 10 m above sea level. The factor of 1% was to account for the wind effect, similar to oil trajectory modeling. The surface current data were obtained from the daily output of the Hybrid Coordinate Ocean Model (HYCOM) surface currents, and surface wind velocities were downloaded from the National Centers for Environmental Prediction Reanalysis

(NCEP). A Runge-Kutta 4th-order method was used to estimate the successive particles locations with a 30-mintue time step.

We modeled *Sargassum* change rate (for both growth and mortality) using a sequence of satellite-detected *Sargassum* distribution images (*25*). The change rate was used to simulate the biological change terms during the physical transport modeling. Basically, we estimated the *Sargassum* change rates from the satellite-derived monthly mean *Sargassum* abundance maps, and associated the change rates with their corresponding environmental conditions. This way, the change rate can be modeled from the environmental factors using a Random Forest regression (*25*). The mean change rate at successive locations of each time step was applied to calculate the *Sargassum* abundance changes during the transport.

Simulating the Great Atlantic *Sargassum* Belt (GASB) pattern formation

To simulate the *Sargassum* transport and abundance changes under average environmental conditions, we applied the mean HYCOM surface currents, NCEP winds, and *Sargassum* change rates from 2011-2015 in the bio-physical model to investigate the large-scale GASB pattern formation. The monthly mean *Sargassum* distributions were the averaged MODIS maps in recent bloom years (2011-2012 and 2014-2017).

Because winter-spring blooms typical started in the Central Atlantic in earlier months, particles were released and assigned initial weights (density), and were then tracked forward from January and April for six and three months, respectively, to July under the average environmental conditions to investigate the July GASB pattern formation. In these experiments, we tracked the *Sargassum* particles under three different scenarios: 1) *Sargassum* particles were initiated uniformly in the Central Atlantic in January (Fig. S1A). The total *Sargassum* abundance was the same as in the satellite observations in January. 2) *Sargassum* particles were initiated according to the satellite-derived mean distributions in the Central Atlantic in January (Fig. S1B). 3) *Sargassum* particles were initiated according to the satellite-derived mean distributions in the Central Atlantic in April (Fig. S1C). In each of the three scenarios, *Sargassum* change rate was either used or not used in the model in order to contrast the results and to test the significance of biological growth and mortality in determining the GASB distributions.

Assessing the regional connectivity across the Atlantic Ocean

We used forward and backward tracking to investigate the regional connectivity of *Sargassum* particles in different parts of the Atlantic Ocean and to test the main sources (Fig. S2). Here, regional connectivity was quantified as the percent of *Sargassum* particles in one end region (R_E) that are tracked from another potential source region (R_S). Specifically, regional connectivity $Con_{R_S R_E}^{T_S T_E}$ represents the percent of particles located in region R_E at time T_E which come from region R_S at time T_S (regardless of forward tracking or backtracking):

$$Con_{R_S R_E}^{T_S T_E} = \frac{N_{R_S R_E}^{T_S T_E}}{N_{R_E}^{T_E}} \times 100\% \quad (1)$$

where T_S is earlier than T_E, $N_{R_E}^{T_E}$ represents the number of particles in region R_E at time T_E while $N_{R_S R_E}^{T_S T_E}$ represents the number of particles in region R_E at time T_E and tracked back to region R_S at time T_S.

Deriving *Sargassum* growth and mortality rate (i.e., change rate) from satellite observations

We estimated the *Sargassum* change rate from the monthly distributions of *Sargassum* biomass density using the following equation:

$$Rate = \frac{log_2(W_t/W_i)}{t} \quad (2)$$

where t is the number of days between adjacent months, W_t is the total mean biomass in the later month (t days after the initial month), W_i is the total mean biomass in the initial month. The unit of the derived change rate is doublings per day. The rate is assigned to be the change rate in the later month. For example, the change rate derived from the mean biomass in November and December is referred to as the change rate in December in this study.

Measuring the agreement between the modeling results and observations

The overall agreement between observations and the modeled *Sargassum* distributions was evaluated using the matchup percentage of *Sargassum* abundance ($abundance_{\text{match}}$) after weighting the particles with their areal densities:

$$abundance_{match} = \frac{\sum_{i=0}^{i=N_{match}} f_i}{\sum_{i=0}^{i=N_{obs}} f_i} \times 100\% \quad (3)$$

where the subscript *obs* and *match* represent the pixels from valid MODIS observations and the matchup pixels where both the observations and the model outputs indicate *Sargassum* presence, respectively. f_i is the *Sargassum* areal density at pixel i.

Analyzing environmental conditions and their impacts on the inter-annual variations of *Sargassum* blooms

We analyzed the Sea Surface Temperature (SST), Chlorophyll-a (Chl) concentration, and dust deposition rate to investigate their potential impacts on the inter-annual variations of the *Sargassum* blooms. The data descriptions are summarized in Table S1. The daily outputs were averaged to monthly means for this analysis. The Amazon discharge rate at the Obidis station was also downloaded from the HYBAM dataset to examine the riverine nutrient impacts.

[**Nutrient availability**]

Direct measurements of water-column dissolved nutrients in the Central West Atlantic were only available in 2010 and 2018. We measured the concentrations of dissolved inorganic nutrients on two cruises to the Amazon Plume region: cruise KN197 (22 May – 24 June 2010) and cruise

EN614 (8 May – 1 June 2018), with stations and cruise track guided by satellite imagery and hydrographic measurements to sample the Amazon plume and surrounding waters (*42*). On both cruises, we used a CTD-rosette system to collect water samples, supplemented by samples collected from a flow-through system, and measured nutrient concentrations (NO_3^- + NO_2^-, PO_4^{3-}, SiO_2) at sea using a Lachat QuickChem 8000 FIA system.

In other years, direct measurements of nutrients in the Central West Atlantic were not available. Therefore, we used several indicators to infer possible nutrient availability. These include the annual deforestation and fertilizer consumption in Brazil as well as satellite-derived Chl and SST anomalies (CHLA and SSTA) in the Central West Atlantic. In the tropical Atlantic Ocean, light is not a limiting factor, therefore CHLA could reflect the nutrient availability. As upwelling brings deep, cold but nutrient-rich water to the surface, SSTA has been used as an upwelling index and can be indicative of the amount of nutrients from upwelling (*37*). We recognized that lower SST could also be a result of reduced solar insolation due to dust layers (*43*). In such cases, lower SST is not associated with increased nutrients, and therefore not associated with positive CHLA. For example, the extremely low SST in the Central East Atlantic in early months of 2012 could be partially due to the higher dust plume (as indicated by the modeled dust deposition rate in Fig. S3B) as opposed to upwelling, which could explain why CHLA is not significantly higher in spring 2012 than in other years. In the following analyses, the nutrient level is mostly inferred from CHLA and SSTA, but in the Central West Atlantic nutrient input is also inferred from the Amazon River discharge anomaly in addition to CHLA.

[**Mean environmental conditions and correlation analyses**] For each satellite-derived monthly *Sargassum* change rate, we generated the mean environmental conditions using SST, Chl, and other variables of the two adjacent months from which the change rate was estimated. The mean condition for an environmental variable for each month was defined as the mean value weighted by the *Sargassum* areal density:

$$Var = \frac{\sum_{i=1}^{N} Var_i Density_i}{\sum_{i=1}^{N} Density_i} \tag{4}$$

where i is the pixel index, N is the number of pixels with positive *Sargassum* density during that month, Var_i is the variable value at pixel i, and $Density_i$ is the *Sargassum* areal density at pixel i. Correlation analyses were then conducted for the months of interest between different years to test the potential impacts of the environmental factors on *Sargassum* growth and mortality in certain growth phases using these mean environmental variables.

[**Separate analyses in the Central West Atlantic and Central East Atlantic during winter**] As shown in Fig. 1B, winter blooms typically exist in both the western and eastern sides of the central Atlantic. Considering the distinct environmental conditions of these two regions, the Central West Atlantic and Central East Atlantic were analyzed separately in Fig. S7A & S7B. The Central East Atlantic is defined from 0° N - 12° N and 35° W - 15° W, while the Central West Atlantic is defined from 9° N - 19° N and 58° W - 33° W during these correlation analyses.

Supplementary Text

Climatological *Sargassum* distributions

The recent *Sargassum* distributions have strong seasonal patterns (Fig. 1B). In January, *Sargassum* was mostly observed within the Central Atlantic, located in both the Central West Atlantic and Central East Atlantic. They served as two potential seed populations for the subsequent spring-summer blooms. From January to April, *Sargassum* developed into a bloom extending to the tropical Atlantic and some of the *Sargassum* may have already reached the Caribbean islands. After April, the bloom continued to develop until the GASB was well formed in July, extending northwestward by the North Brazil Current (NBC) and North Equatorial current (NEC) and eastward to the West Africa coast by the North Equatorial Counter Current (NECC, Fig S2A). In the following months, the strong NECC continued to bring the *Sargassum* aggregations to the eastern Atlantic while the *Sargassum* abundance began to decrease, leading to the gradual dissipation of the GASB from September to October (Fig. 1B). During the boreal winter, large *Sargassum* mats in the Central East Atlantic and Central West Atlantic could diminish (such as in 2012) or contribute to new blooms in the coming year (such as in 2014 – 2017). In December 2012, *Sargassum* mostly disappeared in the tropical Atlantic, and therefore there was no bloom in 2013.

GASB pattern formation – impact of initial *Sargassum* distributions

Because *Sargassum* mats can be very small, satellite sensors will inevitably miss small mats. However, even if the same amount of satellite-observed *Sargassum* were uniformly distributed in the Central Atlantic, they would still concentrate in the GASB zone in summer months (Fig. S1A). This suggests regardless of the initial *Sargassum* distributions and regardless of whether satellites missed those small *Sargassum* mats, the general GASB patterns can always form in summer months under physical and biological processes. Additionally, the July GASB patterns are better reproduced when satellite-derived *Sargassum* distributions in later months (e.g., April) than in January were used to initialize the simulation (Fig. S1C). This is because of the reduced error accumulations from the physical locations and biological change terms when the simulation was performed in a shorter period.

Role of increased nutrient supply from the Amazon River discharge

Compared to 2002, the mean total forest loss in the Brazilian Amazon River basin increased by ~ 25% and the total fertilizer consumption in Brazil increased by ~ 67% in the period of 2011 – 2018 (Figs. S4A & S4B). Some of the excessive fertilizers are likely to end up in the river water discharged to the Central West Atlantic. Together with increased deforestation, nutrient concentrations in the Amazon River plume may have increased in recent years as a consequence of the expanded human activities including deforestation, agriculture, and other developments. A comparison of surface nutrient concentrations measured in the Amazon plume region in spring 2010 and spring 2018 provides direct observation for increased delivery of nitrate and phosphate to the Central West Atlantic (Figs. S4E & S4F). Both nitrate and phosphate concentrations were higher in 2018 than in 2010 across a broad range of salinities reflecting the interaction and mixing of the river plume with surrounding oceanic waters. In contrast, silicate concentrations showed the same dependence on salinity in both 2010 and 2018 (Fig. S4G), implying that the contrast in nitrate and phosphate is a result of increased inputs from the river rather than a difference in vertical or horizontal mixing between years.

Previous studies of the Mississippi River plume have found that the nutrient flux is proportional to the river flow flux (*44*). It is reasonable to expect the same for the Amazon River. However, because of the possibly increased nutrient concentrations, nutrient flux may be disproportionally higher than predicted by river volume flux. One observation supporting this argument is that, compared to the very low dissolved nutrient and phytoplankton in the Amazon River plume in the 1960s (*45*), much higher chlorophyll concentration was measured in the plume region in recent years (*31, 46*). Independent from these field-based observations, mean chlorophyll near the Amazon derived from satellite measurements also suggests enhanced nutrient supply in recent years (Fig. S4C).

Compared to the mean discharge rate during peak seasons (200,000 m^3/s), the Amazon River discharge anomaly may appear relatively small (~10%), but the magnitude of this anomaly (~ 20,000 m^3/s, Fig. 2B) is indeed large and even comparable to the mean flow of the Mississippi River (Fig. S6D). The discharge from the Mississippi River is believed to be a major nutrient source to nourish the major *Sargassum* blooms in the Gulf of Mexico.

Therefore, the observed higher-than-normal Amazon River discharge, together with increased human activities (deforestation, fertilizer use) could play a major role in driving the recent blooms in the tropical Atlantic.

Water temperature and *Sargassum* growth

Although it has been widely hypothesized that recent *Sargassum* blooms could be due to global warming, our satellite-based results suggest the opposite, where higher temperature is associated with slower *Sargassum* growth. The temperature inhibition effect alone may be small, as indicated in the previous lab experiment showing small variations at 18 – 30 °C under nutrient enriched conditions (Fig. S5A). It is likely that in the real environment the water temperature is strongly related to nutrient availability (*47*), thus also attributing to the observed high correlations between SST and *Sargassum* growth.

Fig. S6A and S6E show *Sargassum* change rate and SST in the 12 climatological months in the Central Atlantic. Significant negative correlations were found between the two during November and December for both Central West Atlantic (Fig. S7A) and Central East Atlantic (Fig. S7B). In 2014 and 2017, *Sargassum* grew rapidly in the Central West Atlantic in November – to December when mean SST was much lower than in other years (Fig. S7A). This cooler water could be associated with higher nutrients from upwelling or river inputs, thus leading to higher *Sargassum* growth.

Regional connectivity of *Sargassum* blooms in the Caribbean Sea

From Fig. S2C, we found that the majority of the summer *Sargassum* in the Caribbean Sea can be traced back to the Central Atlantic region, while the other regions (such as the North Atlantic and West Africa) show very weak connections with Central Atlantic. In addition to the main source from the Central Atlantic, small amount of *Sargassum* may recirculate within the Caribbean Sea and contribute to the summer bloom in the Caribbean Sea.

Sargassum **blooms seasonality and possible drivers**

Before 2011, most of the *Sargassum* was found in the Gulf of Mexico and Sargasso Sea. *Sargassum* abundance increases in the winter/spring months in the Gulf of Mexico, followed by transport to the Sargasso Sea where abundance peaks in July to August (*5, 6*; Fig. S6). After 2011, large *Sargassum* blooms developed in the Central Atlantic, with abundance peaking in June/July (Fig. 3B) and positive change rate during first half of the year (Fig. S6).

In both Gulf of Mexico and tropical Atlantic, similar seasonal patterns in change rate were observed (positive in the first half of the year, Fig. S6), which may be a result of **changing nutrient availability** and **the biological cycle of *Sargassum***. In the Sargasso Sea, *Sargassum* seasonality may be largely attributed to **physical aggregations** of the *Sargassum* seed populations from the other two regions (Gulf of Mexico and tropical Atlantic) from June to November. In later months limited nutrients may hinder *Sargassum* growth, resulting in decreased abundance in the Sargasso Sea during winter - spring.

Although we are unaware of any relevant work on the *Sargassum* internal cycle, previous studies have shown that the free-running **circannual rhythms** (CR) do exist in other brown seaweed species (*35*). Thus, it is likely that *Sargassum* also has endogenous CR, which control their growth patterns regardless of the external conditions (*Dr. Klaus Lüning, Alfred Wegener Institute for Polar and Marine Research, personal communication*). In addition, the **seasonality in nutrient supply** could also contribute to the observed seasonality in *Sargassum* change rate (Figs. S6A &S6B). In both Gulf of Mexico and tropical Atlantic, significant positive correlations were found between *Sargassum* change rate and corresponding **river discharge** (Figs S6C & S6D). Strong correlations between **water temperature** and *Sargassum* change rate (Figs S6E & S6F) were also observed, although these correlations may simply be a coincidence as water temperature also co-varied with other environmental factors such river discharge. In the tropical Atlantic, other nutrient sources include **West Africa upwelling, dust deposition, and equatorial upwelling,** which all show strong seasonality. Therefore, the observed seasonality in *Sargassum* abundance and growth rate could be a result of both *Sargassum*'s inherent circannual rhythms and seasonality in nutrient availability.

Figures

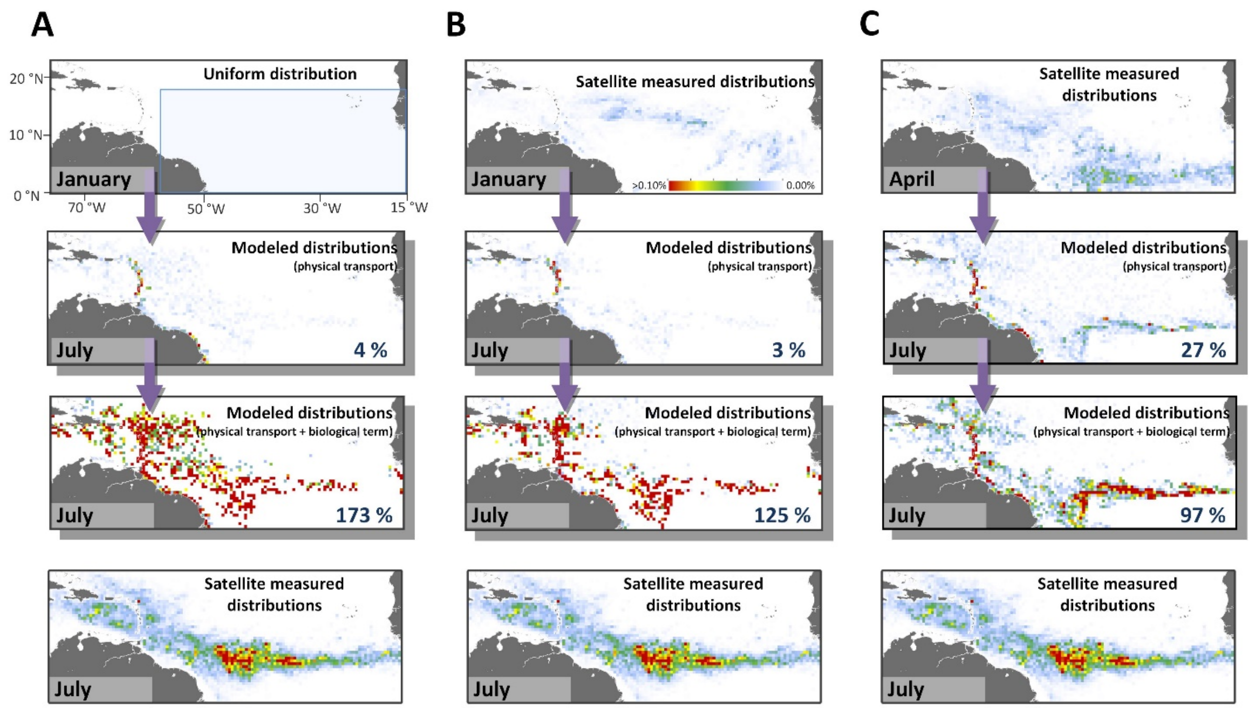

Fig. S1.

The GASB pattern formation in July (climatological month). (**A**) Forward tracking from January to July, when a uniform *Sargassum* distribution (bounded by the blue lines: 5° S -18 ° N and 58° W - 15° W) in January was used to initialize the model. The total integrated *Sargassum* amount is the same as the MODIS-derived value in January. (**B**) Forward tracking from January to July when *Sargassum* in January from MODIS observations was used to initialize the model. (**C**) Same as in (B), but *Sargassum* in April from MODIS observations was used to initialize the model. The matchup percentages of the modeled results with the corresponding satellite observations are annotated in the bottom right corner of each image, where a 100% matchup represents good agreement.

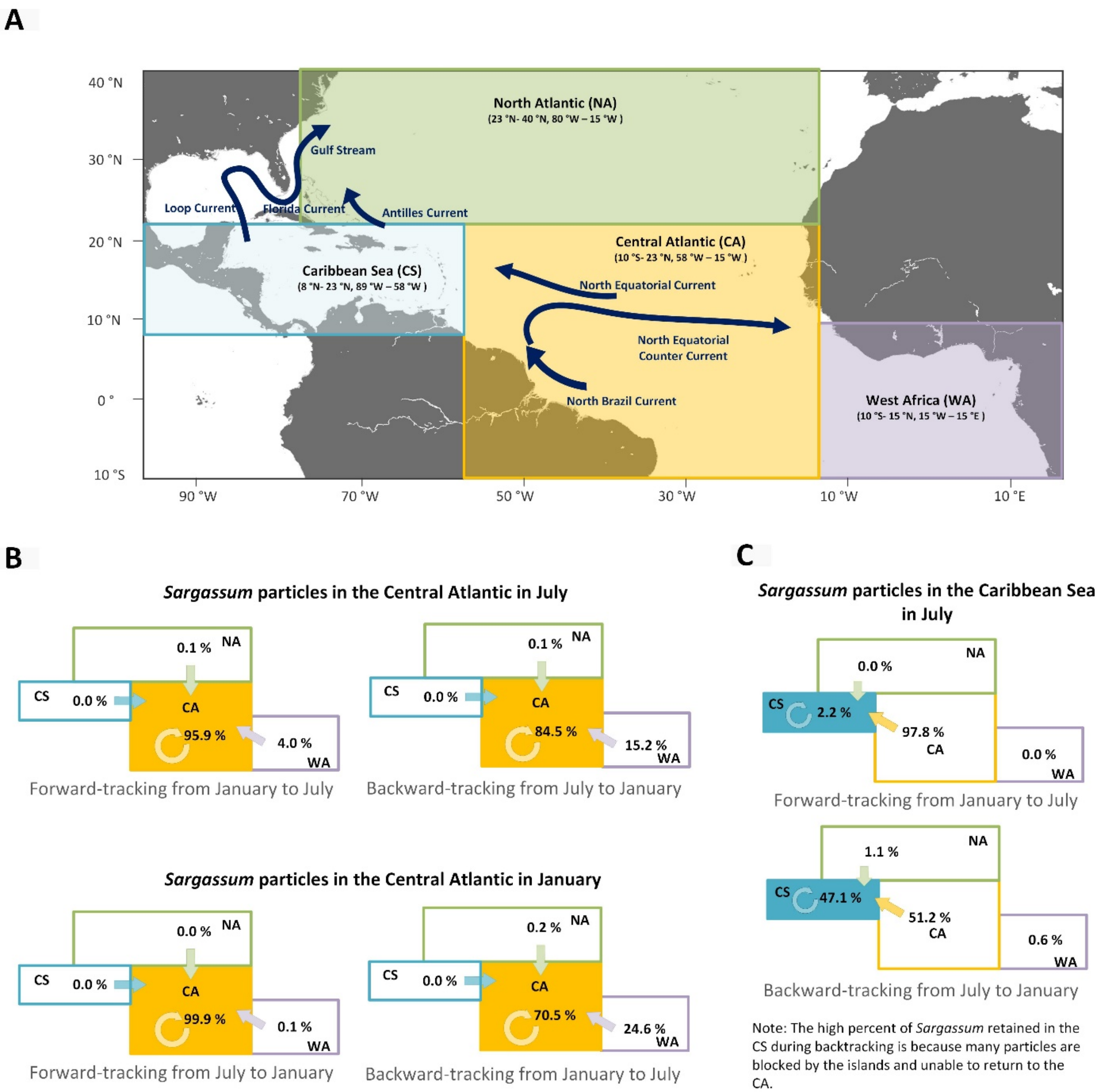

Fig. S2.

***Sargassum* regional connectivity in the Caribbean Sea and Atlantic Ocean.** (**A**) The geographic coverage of the Central Atlantic, Caribbean Sea, North Atlantic, and West Africa. The major ocean currents discussed in this study are annotated with dark blue arrows. (**B**) The regional connectivity of *Sargassum* bloom sources in the Central Atlantic in July and January, determined from forward and backward tracking for six months. (**C**) The regional connectivity of *Sargassum* bloom sources in the Caribbean Sea in July, determined from forward and backward tracking for six months. The percentages in (**B**) and (**C**) represent the fraction of *Sargassum* particles that entered the highlighted region (the end arrow) from the marked area (the begin arrow) six months earlier (see definitions in equation (1)).

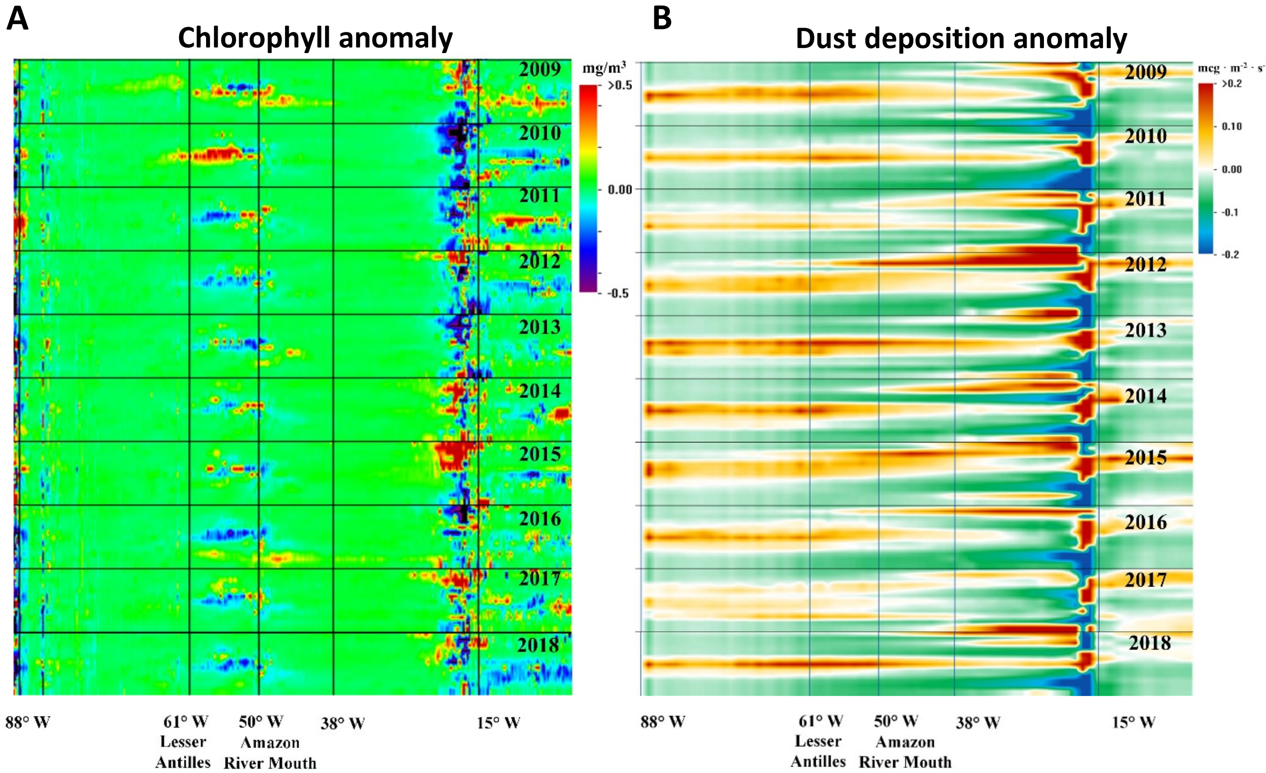

Fig. S3.

The latitude-averaged monthly mean chlorophyll-a and dust deposition anomaly from 2009 to 2018. The vertical lines marked at 88° W, 61° W, 50° W, 38° W, and 15° W represent the Yucatan peninsula coast, Barbados coast, the Amazon River month, the middle of the central Atlantic, and the West Africa coast, respectively.

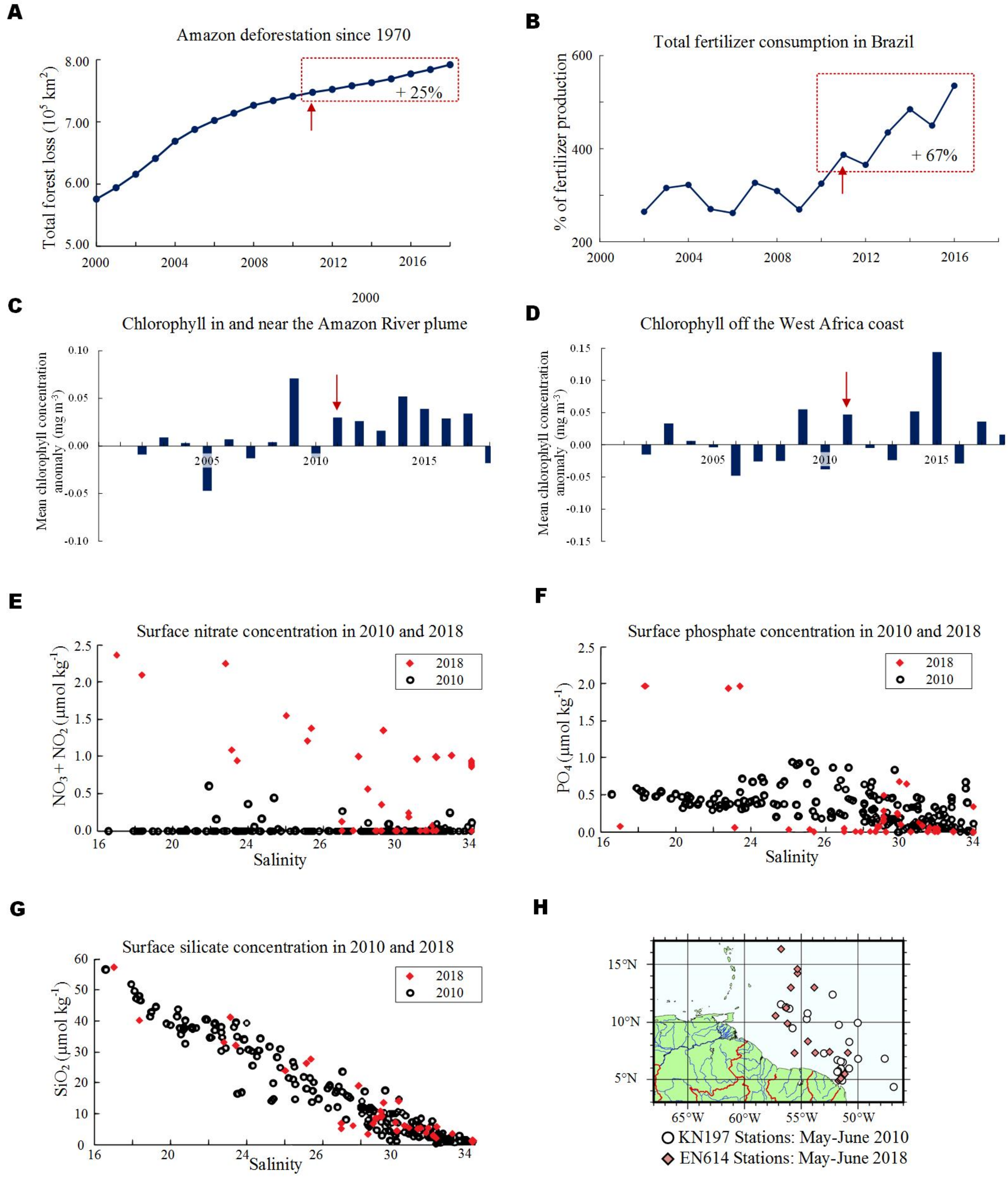

Fig. S4.

Observations of the potentially enhanced nutrient supply in recent years in both Central West Atlantic and Central East Atlantic. (**A**) The total Amazon forest loss since 1970. (Data only include the Brazilian Amazon, based on estimates provided by the Brazilian National Institute of Space Research and the United Nations Food and Agriculture Organization, downloaded at https://rainforests.mongabay.com/amazon/deforestation_calculations.html). (**B**) The total fertilizer consumption in Brazil (Data from World Development Indicators, Food and Agriculture Organization). The numbers marked inside the red dashed boxes in (**A** and **B**) represent the percent increase of the mean values in the boxes compared to the data in 2002. (**C** and **D**) The annual mean chlorophyll anomaly measured in and near the Amazon River plume and off the West Africa coast. The region in and near the Amazon River plume is defined from 10° S - 10° N and 50° W - 25° W. The region off the West Africa coast is defined from 0° N - 12° N and 35° W - 15° W. The red arrows indicate the year of 2011 when large *Sargassum* amount first appeared in the Caribbean and tropical Atlantic. (**E - G**) Surface concentration of nitrate, phosphate, and silicate during cruises KN197 (circles, 22 May – 24 June 2010) and EN614 (red diamonds, 8 May – 1 June 2018) as a function of salinity. (**H**) Hydrographic stations sampled during cruise KN297 (circles) and EN614 (red diamonds). During cruise KN197, samples were also collected from the ship's flowing seawater system (*42*).

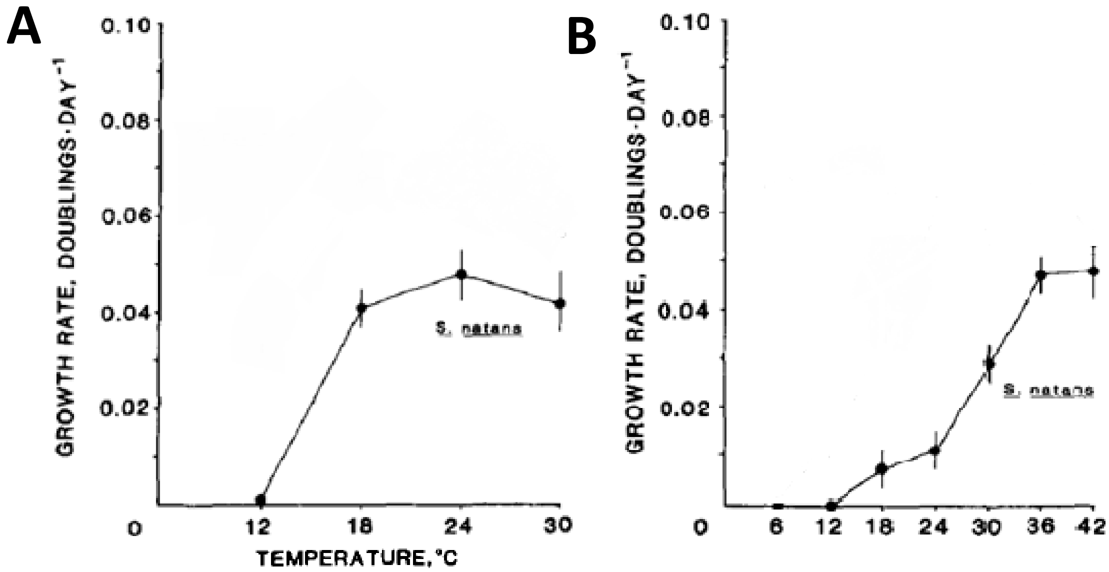

Fig. S5.

Specific growth rate (doublings per day) of *Sargassum natans* under different water temperature (A) and salinity (B) under nutrient-rich conditions. *Sargassum fluitans,* the other type of pelagic *Sargassum* which is also present in our study region, is found to have similar responses to temperature and salinity changes. The vertical bars indicate standard errors from 6 measurements. Note the decrease in growth rate when temperature is > 24ºC. Such temperature-induced inhibition becomes very strong once temperature is above 30ºC. When salinity is reduced to 30 from 36, the growth rate of both *Sargassum natans* and *fluitans* can decrease by ~50%. The plots and observations of the salinity and temperature responses of *Sargassum fluitans* and *natans* listed above are all from Hanisak & Samuel (*1987*). Because *Sargassum* typically lives in nutrient-poor open-ocean waters, stronger temperature responses observed from this study can possibly be due to the poor nutrient availability than in the laboratory experiments.

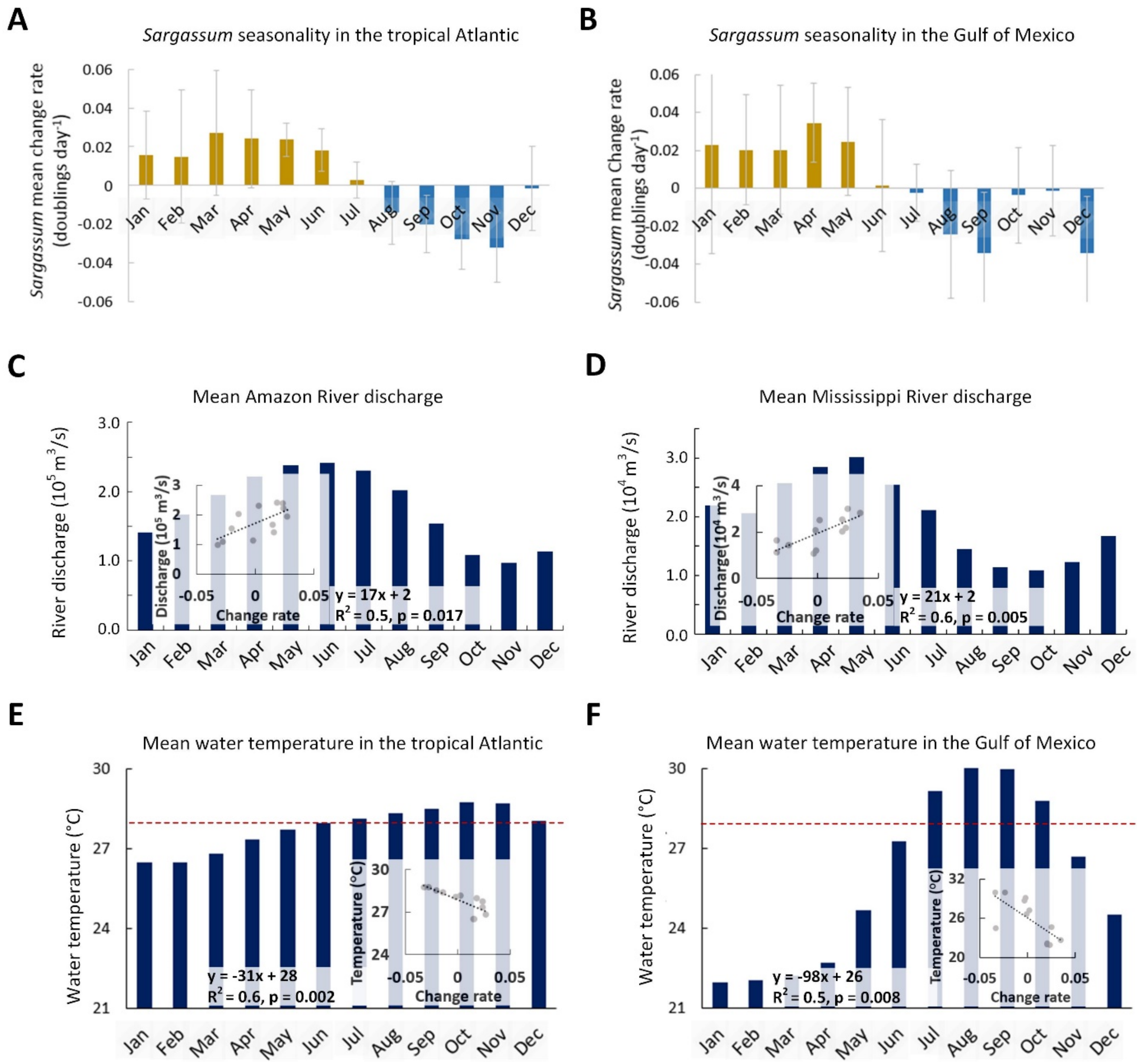

Fig. S6.

Seasonality of mean *Sargassum* change rate (A & B), mean river discharge (C & D), and mean water temperature (E & F) in the Gulf of Mexico and tropical Atlantic. The inserted small figures and equations in C-F show the correlation analyses of the corresponding variables with the *Sargassum* change rate in the region. The red dashed lines indicate water temperature of 28 °C.

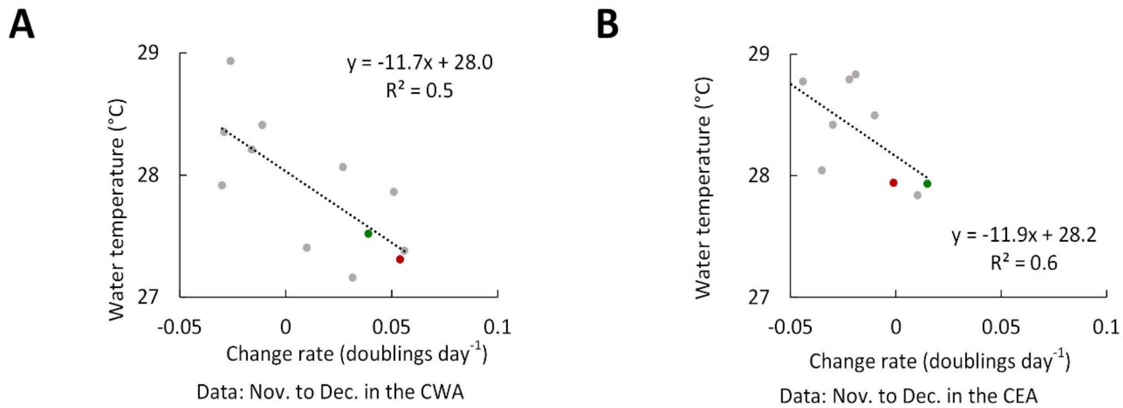

Fig. S7.

Correlations between *Sargassum* change rate and mean SST during November –December in the Central West Atlantic and Central East Atlantic (**A** and **B**), respectively. The data from December 2017 and 2014 are marked in green and red, respectively.

Table S1.
Environmental datasets used to investigate the potential environmental impacts on *Sargassum* growth and mortality in different years.

Environmental variable name	Source	Temporal resolution	Spatial resolution
SST	Multi-scale Ultra-high Resolution (MUR) SST https://mur.jpl.nasa.gov/index.php	Daily	0.01°
Chl concentrations	NASA Ocean Color MODIS Aqua (https://oceancolor.gsfc.nasa.gov/)	Monthly	4 km
Dust deposition rate	Spectral Radiation-Transport Model for Aerosol Species (SPRINTARS) model version 5.9.0 (*48*)	Daily	1.125°

Table S2.

Hypotheses and observations on the inter-annual variations of *Sargassum* change rate during both growth and decrease phases since 2011. Note that the term "dust" refers to wet deposition of the African dust unless noted otherwise. The Amazon biomass burning induced dust occurs during July – November could limit light (*49, 50*), but the overall impacts should be small, as the light availability (as estimated from the MODIS monthly data products of photosynthetically active radiation (PAR)) across the Central Atlantic did not show significant changes during recent years.

<table>
<tr><td rowspan="12">2011</td><td colspan="2">Growth phase:</td></tr>
<tr><td colspan="2">Fast early growth since April</td></tr>
<tr><td>Causes</td><td>Observations</td></tr>
<tr><td>➢ Sargassum seeds from previous years</td><td>➢ Movie. S1</td></tr>
<tr><td>➢ Nutrients accumulation from Amazon during 2009 – 2010</td><td>➢ Higher Amazon River discharge from 2008-2009 (Fig.2B)
➢ Higher CHLA near the Amazon River mouth during 2009 – 2010</td></tr>
<tr><td>➢ Enhanced nutrients from upwelling in the Central East Atlantic in 2009</td><td>➢ Higher CHLA and lower SSTA near the West Africa in 2009</td></tr>
<tr><td>➢ Lower SST compared to 2010</td><td>➢ Fig. 2D</td></tr>
<tr><td colspan="2">Decrease phase:</td></tr>
<tr><td colspan="2">Normal decrease</td></tr>
<tr><td>Causes</td><td>Observations</td></tr>
<tr><td>➢ Normal water temperature during later summer to winter of 2011</td><td>➢ Fig. 2D</td></tr>
</table>

<table>
<tr><td rowspan="10">2012</td><td colspan="2">Growth phase:</td></tr>
<tr><td colspan="2">Normal early growth since winter 2011</td></tr>
<tr><td>Causes</td><td>Observations</td></tr>
<tr><td>➢ Sargassum seeds from winter 2011</td><td>➢ Movie. S1</td></tr>
<tr><td>➢ Enhanced nutrients from upwelling in the Central East Atlantic in 2012</td><td>➢ Higher CHLA and lower SSTA near the Central East Atlantic from winter 2011 to spring 2012
➢ Note that the extremely low SST in the eastern Atlantic in early months could be partially due to the higher dust plume as opposed to upwelling (Fig. S3B)</td></tr>
<tr><td>➢ Lower SSTA during the growth phase</td><td>➢ Fig. 2D</td></tr>
<tr><td colspan="2">Decrease phase:</td></tr>
<tr><td colspan="2">Rapid decrease</td></tr>
<tr><td>Causes</td><td>Observations</td></tr>
</table>

	➢ Overall, lower nutrients across the central Atlantic in the summer to winter months	➢ Lower Amazon River discharge from 2010 – 2011 (Fig. 2B) ➢ Lower CHLA near the Amazon River plume region in 2012
	➢ Higher water temperature since late summer of 2012	➢ Fig. 2D

2014	**Growth phase:**	
	Fast growth near the Central East Atlantic since January	
	Causes	Observations
	➢ Cooler water temperature since autumn 2013 favorable for early growth	➢ Fig. 2D
	➢ Enhanced nutrients from upwelling in the Central East Atlantic in 2014	➢ Higher CHLA and lower SSTA near the Central East Atlantic from winter 2013 to spring 2014
	➢ Higher riverine nutrients from Amazon River discharge from 2013-2014	➢ Higher Amazon River discharge anomaly accumulated from 2013 – 2014 (Fig. 2B) ➢ Positive CHLA near the Amazon River mouth during 2013 to 2014
	Decrease phase:	
	Slow decrease	
	Causes	Observations
	➢ Higher nutrients from Amazon River and upwelling processes in 2014	➢ See above
	➢ Lower water temperature from the summer to winter of 2014	➢ Fig. 2D

2015	**Growth phase:**	
	Moderate growth across the entire central Atlantic	
	Causes	Observations
	➢ Lots of *Sargassum* seeds from winter 2014	➢ Movie. S1
	➢ Enhanced nutrients from upwelling in the Central East Atlantic in 2015	➢ Higher CHLA and lower SSTA near the Central East Atlantic from winter 2014 to spring 2015
	➢ Still high riverine nutrients from Amazon River discharge in 2015	➢ Higher Amazon River discharge anomaly accumulated from 2014 – 2015 (Fig. 2B) ➢ Positive CHLA near the Amazon River mouth during 2014 to 2015
	➢ The significant *Sargassum* biomass requires more nutrients thereby lower down the overall growth rate	➢ Movie. S1 and Fig. 3A
	Decrease phase:	

Year	Causes	Observations
	Fast decrease and most *Sargassum* dead near the Central West Atlantic before February 2016	
	Causes	Observations
	➢ Nutrient limitation due to the large *Sargassum* standing stock	➢ See above
	➢ Warmer water temperature since winter 2015	➢ Fig. 2D
2016	**Growth phase:**	
	Moderate growth near the Central East Atlantic	
	Causes	Observations
	➢ Small amount of *Sargassum* seeds near the Central East Atlantic from winter 2015	➢ Movie. S1
	➢ Relatively lower nutrients from upwelling in the Central East Atlantic in 2016 compared to that in 2014-2015	➢ Relatively lower CHLA and higher SSTA near the Central East Atlantic compared to the conditions in 2014-2015
	➢ Lower riverine nutrient from Amazon River in spring to summer 2016	➢ Lower Amazon River discharge anomaly in 2016 (Fig. 2B) ➢ Negative CHLA near the Amazon River mouth during spring to summer 2016
	➢ Warmer SST hindered the growth	➢ Fig. 2D
	Decrease phase:	
	Slow decrease during summer to autumn, rapid increase during winter months	
	Causes	Observations
	➢ Nutrient input from river discharge since autumn 2016 transported across the Central Atlantic	➢ Higher Amazon River discharge anomaly since winter 2016 ➢ Higher CHLA near Amazon River month in autumn 2016 transported to the Central East Atlantic
	➢ Enhanced nutrients from upwelling near the Central East Atlantic during winter 2016	➢ Higher CHLA near the Central East Atlantic in winter 2016 (Fig. S3A)

Year	Causes	Observations
2017	**Growth phase:**	
	Rapid growth in the winter 2016, moderate growth during spring 2017	
	Causes	Observations
	➢ Lots of *Sargassum* seeds from winter 2016	➢ Movie. S1
	➢ Enhanced nutrients from upwelling in the Central East Atlantic in 2016	➢ Higher CHLA near the Central East Atlantic from winter 2016 to spring 2017
	➢ Enhanced Amazon nutrient input	➢ Positive Amazon River discharge anomaly from 2016 – 2017 (Fig. 2B) ➢ Positive CHLA near the Amazon River mouth during 2017
	➢ Warmer SST hinder the growth during spring, but cooler temperature occurs from summer to winter months	➢ Movie. S1 and Fig. 2D
	Decrease phase:	
	Normal decrease in autumn and rapid growth in winter near the Central West Atlantic	

	Causes	Observations
	➢ Enhanced nutrients	➢ Positive CHLA and negative SSTA near the Central East Atlantic in winter 2017
	➢ Cooler water temperature across the central Atlantic since winter 2017	➢ Fig. 2D

Movie S1. (separate file)
Monthly mean *Sargassum* distributions in the Intra-Americas Sea and Atlantic Ocean from 2000 to 2018.

References and Notes

1. J. N. Butler, B. F. Morris, J. Cadwallader, A. W. Stoner, Studies of *Sargassum* and the *Sargassum* community (Bermuda Biological Station, special publication no. 22, 1983).

2. T. L. Casazza, S. W. Ross, Fishes associated with pelagic Sargassum and open water lacking Sargassum in the Gulf Stream off North Carolina. *Fish Bull.* **106**, 348–363 (2008).

3. B. Witherington, S. Hirama, R. Hardy, Young sea turtles of the pelagic *Sargassum*-dominated drift community: Habitat use, population density, and threats. *Mar. Ecol. Prog. Ser.* **463**, 1–22 (2012). doi:10.3354/meps09970

4. J. N. Butler, A. W. Stoner, Pelagic *Sargassum*: Has its biomass changed in the last 50 years? *Deep Sea Res. Part I Oceanogr. Res. Pap.* **31**, 1259–1264 (1984). doi:10.1016/0198-0149(84)90061-X

5. J. F. Gower, S. A. King, Distribution of floating *Sargassum* in the Gulf of Mexico and the Atlantic Ocean mapped using MERIS. *Int. J. Remote Sens.* **32**, 1917–1929 (2011). doi:10.1080/01431161003639660

6. J. Gower, E. Young, S. King, Satellite images suggest a new *Sargassum* source region in 2011. *Remote Sens. Lett.* **4**, 764–773 (2013). doi:10.1080/2150704X.2013.796433

7. A. S. Maurer, E. De Neef, S. Stapleton, *Sargassum* accumulation may spell trouble for nesting sea turtles. *Front. Ecol. Environ.* **13**, 394–395 (2015). doi:10.1890/1540-9295-13.7.394

8. O. Oyesiku, A. Egunyomi, Identification and chemical studies of pelagic masses of *Sargassum natans* (Linnaeus) Gaillon and *S. fluitans* (Borgessen) Borgesen (brown algae), found offshore in Ondo State, Nigeria. *Afr. J. Biotechnol.* **13**, 1118–1193 (2014). doi:10.5897/AJB2013.12335

9. M. T. M. de Széchy, P. M. Guedes, M. H. Baeta-Neves, E. N. Oliveira, Verification of Sargassum natans (Linnaeus) Gaillon (Heterokontophyta: Phaeophyceae) from the Sargasso Sea off the coast of Brazil, western Atlantic Ocean. *Check List* **8**, 638–641 (2012). doi:10.15560/8.4.638

10. V. Smetacek, A. Zingone, Green and golden seaweed tides on the rise. *Nature* **504**, 84–88 (2013). doi:10.1038/nature12860 Medline

11. C. Hu, B. Murch, B. Barnes, M. Wang, J.-P. Maréchal, J. Franks, D. Johnson, B. Lapointe, D. Goodwin, J. Schell, A. Siuda, *Sargassum* watch warns of incoming seaweed (Eos, 2016); doi:10.1029/2016EO058355

12. M. Wang, C. Hu, Mapping and quantifying *Sargassum* distribution and coverage in the Central West Atlantic using MODIS observations. *Remote Sens. Environ.* **183**, 350–367 (2016). doi:10.1016/j.rse.2016.04.019

13. M. Wang, C. Hu, Predicting *Sargassum* blooms in the Caribbean Sea from MODIS observations. *Geophys. Res. Lett.* **44**, 3265–3273 (2017). doi:10.1002/2017GL072932

14. K. Langin, Mysterious masses of seaweed assault Caribbean islands (2018); https://www.sciencemag.org/news/2018/06/mysterious-masses-seaweed-assault-caribbean-islands.

15. J. Partlow, G. Martinez, Mexico deploys its navy to face its latest threat: Monster seaweed (2015); https://www.washingtonpost.com/world/the_americas/mexico-deploys-its-navy-to-face-its-latest-threat-monster-seaweed/2015/10/28/cea8ac28-710b-11e5-ba14-318f8e87a2fc_story.html?noredirect=on&utm_term=.212b01de8055

16. J. Rawlins-Bentham, *Sargassum*: A National Emergency & Energy Source (2018); http://gisbarbados.gov.bb/blog/sargassum-a-national-emergency-energy-source/

17. *Sargassum* and Oil Spills Monitoring Pilot Project for the Caribbean and Adjacent Regions Workshop; http://www.ioc-unesco.org/index.php?option=com_oe&task=viewEventRecord&eventID=2270

18. French-American workshop on *Sargassum*; www.tamug.edu/mars/tides/

19. J. S. Franks, D. R. Johnson, D. S. Ko, G. Sanchez-Rubio, J. R. Hendon, M. Lay, Unprecedented influx of pelagic *Sargassum* along Caribbean Island coastlines during summer 2011, in *Proceedings of the 64th Annual Gulf and Caribbean Fisheries Institute* (GCFI, 2011), pp. 6–8.

20. J. S. Franks, D. Johnson, D. S. Ko, Retention and growth of pelagic *Sargassum* in the north equatorial convergence region of the Atlantic Ocean: A hypothesis for examining recent mass strandings of pelagic *Sargassum* along Caribbean and West Africa shorelines, in *Proceedings of the 67th Annual Gulf and Caribbean Fisheries Institute* (GCFI, 2014), p. 136.

21. D. Johnson, D. Ko, J. Franks, P. Moreno, G. Sanchez-Rubio, *Proc. Gulf Caribb. Fish. Inst.* **65**, 102–103 (2013).

22. B. E. Lapointe, L. W. Herren, A. Feibel, C. Hu, Evidence of nitrogen-fueled blooms of pelagic *Sargassum* in the Gulf of Mexico, in *Proceedings of the 68th Annual Gulf and Caribbean Fisheries Institute* (GCFI, 2015), pp. 419–420.

23. S. Djakouré, M. Araujo, A. Hounsou-Gbo, C. Noriega, B. Bourlès, On the potential causes of the recent Pelagic *Sargassum* blooms events in the tropical North Atlantic Ocean. *Biogeosciences Discuss.* (2017). doi:10.5194/bg-2017-346

24. M. Wang, C. Hu, J. Cannizzaro, D. English, X. Han, D. Naar, B. Lapointe, R. Brewton, F. Hernandez, Remote sensing of Sargassum biomass, nutrients, and pigments. Geophys. Res. Lett. 45, 12359–12367 (2018).

25. M. Wang, thesis, University of South Florida (2018).

26. See the supplementary materials.

27. J. S. Franks, D. R. Johnson, D. S. Ko, Pelagic *Sargassum* in the Tropical North Atlantic. *Gulf Caribb. Res.* **27**, SC6–SC11 (2016). doi:10.18785/gcr.2701.08

28. M. T. Brooks, V. J. Coles, R. R. Hood, J. F. Gower, Factors controlling the seasonal distribution of pelagic *Sargassum*. *Mar. Ecol. Prog. Ser.* **599**, 1–18 (2018). doi:10.3354/meps12646

29. N. F. Putman, G. J. Goni, L. J. Gramer, C. Hu, E. M. Johns, J. Trinanes, M. Wang, Simulating transport pathways of pelagic *Sargassum* from the Equatorial Atlantic into the Caribbean Sea. *Prog. Oceanogr.* **165**, 205–214 (2018). doi:10.1016/j.pocean.2018.06.009

30. J. M. Schell, D. S. Goodwin, A. N. Siuda, Recent *Sargassum* Inundation Events in the Caribbean: Shipboard Observations Reveal Dominance of a Previously Rare Form. *Oceanography* **28**, 8–10 (2015). doi:10.5670/oceanog.2015.70

31. E. M. Johns, B. A. Muhling, R. C. Perez, F. E. Müller-Karger, N. Melo, R. H. Smith, J. T. Lamkin, T. L. Gerard, E. Malca, Amazon River water in the northeastern Caribbean Sea and its effect on larval reef fish assemblages during April 2009. *Fish. Oceanogr.* **23**, 472–494 (2014). doi:10.1111/fog.12082

32. B. E. Lapointe, A comparison of nutrient-limited productivity in *Sargassum natans* from neritic vs. oceanic waters of the western North Atlantic Ocean. *Limnol. Oceanogr.* **40**, 625–633 (1995). doi:10.4319/lo.1995.40.3.0625

33. B. E. Lapointe, L. E. West, T. T. Sutton, C. Hu, Ryther revisited: Nutrient excretions by fishes enhance productivity of pelagic *Sargassum* in the western North Atlantic Ocean. *J. Exp. Mar. Biol. Ecol.* **458**, 46–56 (2014). doi:10.1016/j.jembe.2014.05.002

34. M. D. Hanisak, M. A. Samuel, Growth rates in culture of several species of *Sargassum* from Florida, USA. *Hydrobiologia* **151**, 399–404 (1987). doi:10.1007/BF00046159

35. K. Lüning, When do algae grow? The third Founders' lecture. *Eur. J. Phycol.* **29**, 61–67 (1994). doi:10.1080/09670269400650501

36. P. C. Pardo, X. A. Padín, M. Gilcoto, L. Farina-Busto, F. F. Pérez, Evolution of upwelling systems coupled to the long-term variability in sea surface temperature and Ekman transport. *Clim. Res.* **48**, 231–246 (2011). doi:10.3354/cr00989

37. T. E. Cropper, E. Hanna, G. R. Bigg, Spatial and temporal seasonal trends in coastal upwelling off Northwest Africa, 1981–2012. *Deep Sea Res. Part I Oceanogr. Res. Pap.* **86**, 94–111 (2014). doi:10.1016/j.dsr.2014.01.007

38. P. Baker, U. Minzlaff, A. Schoenle, E. Schwabe, M. Hohlfeld, A. Jeuck, N. Brenke, D. Prausse, M. Rothenbeck, S. Brix, I. Frutos, K. M. Jörger, T. P. Neusser, R. Koppelmann, C. Devey, A. Brandt, H. Arndt, Potential contribution of surface-dwelling *Sargassum* algae to deep-sea ecosystems in the southern North Atlantic. *Deep Sea Res. Part II Top. Stud. Oceanogr.* **148**, 21–34 (2017). doi:10.1016/j.dsr2.2017.10.002

39. D. Resiere, R. Valentino, R. Nevière, R. Banydeen, P. Gueye, J. Florentin, A. Cabié, T. Lebrun, B. Mégarbane, G. Guerrier, H. Mehdaoui, *Sargassum* seaweed on Caribbean islands: An international public health concern. *Lancet* **392**, 2691 (2019). doi:10.1016/S0140-6736(18)32777-6 Medline

40. C. Hu, A novel ocean color index to detect floating algae in the global oceans. *Remote Sens. Environ.* **113**, 2118–2129 (2009). doi:10.1016/j.rse.2009.05.012

41. M. Wang, C. Hu, On the continuity of quantifying floating algae of the Central West Atlantic between MODIS and VIIRS. *Int. J. Remote Sens.* **39**, 3852–3869 (2018). doi:10.1080/01431161.2018.1447161

42. S. C. Weber, E. J. Carpenter, V. J. Coles, P. L. Yager, J. Goes, J. P. Montoya, Amazon River influence on nitrogen fixation and export production in the western tropical North Atlantic. *Limnol. Oceanogr.* **62**, 618–631 (2017). doi:10.1002/lno.10448

43. J. C. Lehrter, D. S. Ko, M. C. Murrell, J. D. Hagy, B. A. Schaeffer, R. M. Greene, R. W. Gould, B. Penta, Nutrient distributions, transports, and budgets on the inner margin of a river-dominated continental shelf. *J. Geophys. Res. Oceans* **118**, 4822–4838 (2013). doi:10.1002/jgrc.20362

44. J. H. Ryther, D. W. Menzel, N. Corwin, Influence of the Amazon River outflow on the ecology of the western tropical Atlantic. I. Hydrography and nutrient chemistry. *J. Mar. Res.* **25**, 69–83 (1967).

45. J. I. Goes, H. R. Gomes, A. M. Chekalyuk, E. J. Carpenter, J. P. Montoya, V. J. Coles, P. L. Yager, W. M. Berelson, D. G. Capone, R. A. Foster, D. K. Steinberg, A. Subramaniam, M. A. Hafez, Influence of the Amazon River discharge on the biogeography of phytoplankton communities in the western tropical north Atlantic. *Prog. Oceanogr.* **120**, 29–40 (2014). doi:10.1016/j.pocean.2013.07.010

46. D. Kamykowski, S. J. Zentara, Predicting plant nutrient concentrations from temperature and sigma-t in the upper kilometer of the world ocean. *Deep Sea Res. Part I Oceanogr. Res. Pap.* **33**, 89–105 (1986). doi:10.1016/0198-0149(86)90109-3

47. T. Takemura, H. Okamoto, Y. Maruyama, A. Numaguti, A. Higurashi, T. Nakajima, Global three-dimensional simulation of aerosol optical thickness distribution of various origins. *J. Geophys. Res. Atmos.* **105**, 17853–17873 (2000). doi:10.1029/2000JD900265

48. G. R. Foltz, M. J. McPhaden, Impact of Saharan Dust on Tropical North Atlantic SST. *J. Clim.* **21**, 5048–5060 (2008). doi:10.1175/2008JCLI2232.1

49. L. Gonzalez-Alonso, M. Val Martin, R. A. Kahn, Biomass-burning smoke heights over the Amazon observed from space. *Atmos. Chem. Phys.* **19**, 1685–1702 (2019). doi:10.5194/acp-19-1685-2019

50. J. Burney, V. Ramanathan, Recent climate and air pollution impacts on Indian agriculture. *Proc. Natl. Acad. Sci. U.S.A.* **111**, 16319–16324 (2014). doi:10.1073/pnas.1317275111 Medline